Mn–Si-Catalyzed Synthesis and Tip-End-Induced Room Temperature Ferromagnetism of SiC/SiO2 Core–Shell Heterostructures

ARTICLE *in* THE JOURNAL OF PHYSICAL CHEMISTRY C · NOVEMBER 2008

Impact Factor: 4.77 · DOI: 10.1021/jp807012k

THE JOURNAL OF PHYSICAL CHEMISTRY C

Article

Mn#Si-Catalyzed Synthesis and Tip-End-Induced Room Temperature Ferromagnetism of SiC/SiO Core#Shell Heterostructures

Baodan Liu, Yoshio Bando, Chengchun Tang, Masanori Mitome, Kazunari Yamaura, Eiji Takayama-Muromachi, and Dmitri Golberg

J. Phys. Chem. C, **2008**, 112 (48), 18911-18915 • Publication Date (Web): 06 November 2008

Mn−Si-Catalyzed Synthesis and Tip-End-Induced Room Temperature Ferromagnetism of SiC/SiO_2 Core−Shell Heterostructures

Baodan Liu,*,† Yoshio Bando,‡ Chengchun Tang,†,‡ Masanori Mitome,†,‡ Kazunari Yamaura,§ Eiji Takayama-Muromachi,§ and Dmitri Golberg†,‡

Nanoscale Materials Center, WPI Center for Materials Nanoarchitectonics (MANA), and Superconducting Materials Center, National Institute for Materials Science (NIMS), Namiki1-1, Tsukuba, Ibaraki 305-0044, Japan

Received: August 6, 2008; Revised Manuscript Received: September 11, 2008

SiC/SiO_2 heterostructures were synthesized with catalytic Mn−Si alloy particles via a simple thermal evaporation process. The inner SiC nanowires were crystalline and possessed cubic structures with a large number of structural defects. Outer amorphous ∼15 nm thick layers of SiO_2 were 40−100 nm in diameter. A novel peapod-like silica tubular structure encapsulating Mn−Si alloy particles was also discovered. Magnetic measurements revealed that the Mn−Si catalyzed SiC/SiO_2 nanocable heterostructures exhibited tip-end-induced room temperature ferromagnetism. It is believed that the Mn atoms not only played the role of catalyst, but were also responsible for the existing ferromagnetism at the heterostructure Mn−Si-alloy tip-ends. We envisage that the present novel structures, as well as their interesting magnetic properties, should find applications in a future nanodevice design.

1. Introduction

Recently, extensive efforts have been made to achieve reliable protection of various nanostructured materials with thermally and chemically stable sheathes.[1−3] An insulating and chemically inert protective shield can allow the inner material to display its natural properties that are not affected by an environment. For instance, the syntheses of AlN nanotubes and ZnS nanoarchitectures sheathed with insulating BN layers have been carried out via one- or two-stage processes.[2,3] As an important semiconductor material, SiC has potential applications in electronic devices due to its high thermal conductivity, chemical inertness, and mechanical toughness. Compared with bulk SiC crystals, nanostructured SiC materials have displayed superior properties.[4] To date, various SiC nanostructures have been synthesized via different routes. SiC whiskers were prepared through the evaporation of Si and SiO_2 powder mixtures in a graphite crucible;[5] SiC nanoflowers were fabricated by GaN-catalyzing methane on a Si substrate;[6] SiC nanotubes were made through a "shape memory" synthesis of carbon nanotubes and SiO.[7] SiC nanowires coated with BN layers were also fabricated by Tang et al.[8] During the search of new nanomaterials, metal-particle or alloy-catalyst-assisted methods have been proven to serve as effective routes toward the preparation of various structural types.[9−11] And SiC nanowires catalyzed by Fe and Ni particles have indeed been successfully synthesized.[12,13] As a peer of Fe and Ni, Mn shows unique characteristics such as varying valences and ferromagnetic or antiferromagnetic coupling with neighboring atoms.[14] Previous theoretical studies pointed out that a Si tubular structure doped with Mn atoms could display striking ferromagnetic behavior due to Mn−Si coupling.[14] Similar ferromagnetism might also be expected in Mn- or Mn−Si-catalyzed SiC nanostructures.

In this paper, SiC/SiO_2 core−shell structures catalyzed by Mn−Si alloy particles, as well as novel SiO_2 tubular structures periodically encapsulating Mn−Si particles, were synthesized and their magnetic properties were studied in detail.

2. Experimental Methods

SiC/SiO_2 nanocables were synthesized through heating Si (0.7 g, 99.99%, Wako Chemical Co. Ltd.) and SiO_2 (1.5 g, 99.99%, Wako Chemical Co. Ltd.) powder mixtures (1:1) with a small amount of activated carbon powder (0.2 g, 100 mesh, Aldrich Chemical Co., Inc.) in a conventional induction furnace. A MnO_2 powder (0.2 g, 99.99%, Wako Chemical Co. Ltd.) was added into the initial reactants to serve as a Mn source. The details of the experimental installation can be found elsewhere.[15] The mixture of starting materials was put into a h-BN boat and covered with a graphite inductor acting as a heating element. After reacting at 1600 °C for 1.5 h, under the protection of flowing Ar gas at a rate of 800 standard cubic centimeters per minute (sccm), a gray-white fiber-like powder was formed at the surface of the graphite inductor, near the gas outlet. Morphology observations and structure analyses were performed by means of a scanning electron microscope (SEM, JEOL, JEM-6700F) and a high-resolution field-emission transmission electron microscope (TEM, JEOL, JEM-3000F) with an accelerating voltage of 300 kV. The magnetic properties were measured in a commercial Superconducting quantum interference device (SQUID, Quantum Design, MPMS-XL system).

3. Results and Discussion

A typical low-magnification SEM image of SiC/SiO_2 nanocables is shown in Figure 1a. One can see that the SiC/SiO_2 nanocables exhibit uniform diameters, which are in the range of 20−200 nm, as highlighted in Figure 1b. A length of the SiC/SiO_2 nanocables can be up to tens of micrometers, Figure 1a. The white dots, visible in Figure 1a, correspond to Mn−Si catalyst particles. Generally, the particles are slightly larger than

* Corresponding author. E-mail: baodanliu@gmail.com and Liu.Baodan@nims.go.jp.
† Nanoscale Materials Center.
‡ WPI Center for Materials Nanoarchitectonics.
§ Superconducting Materials Center.

10.1021/jp807012k CCC: $40.75
Published on Web 11/06/2008

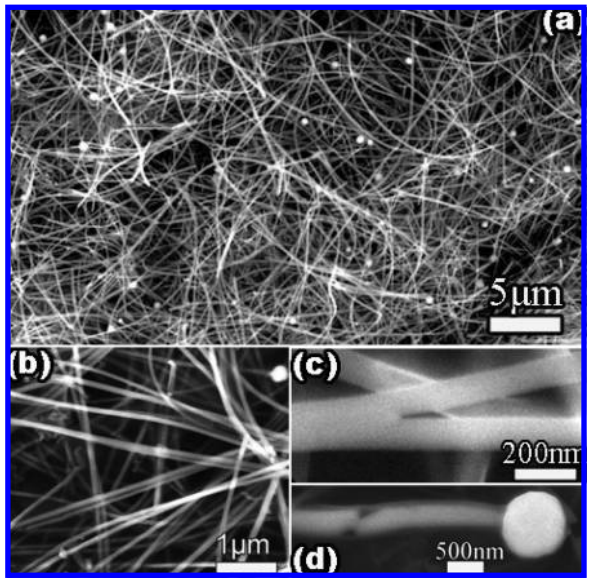

Figure 1. SEM images of SiC/SiO_2 nanocables at (a) low magnification and (b) high magnification; (c) the branched structure of a SiC/SiO_2 nanocable; (d) SiC/SiO_2 nanocables with an encapsulated catalyst particle (internal discontinuous rod is a Mn−Si alloy).

the diameters of cable-like nanowires. An example of a SiC/SiO_2 nanocable with the attached catalyst particle is presented in Figure 1d. The particle has a diameter of ∼1 μm, whereas the nanocable has a diameter of ∼500 nm. The discontinuous rod encapsulated into the SiO_2 tube is made of Mn−Si alloy, which is confirmed by energy dispersive X-ray spectroscopy (EDS). The catalyst alloy particles attached to the tips of SiC/SiO_2 nanocables imply that the well-known vapor−liquid−solid (V-L-S) growth mechanism was in effect during the growth. Figure 1c displays a Y-shape branched structure grown from SiC/SiO_2 nanocables.

To verify the core−shell structures for SiC/SiO_2 nanocables, TEM analysis was performed. Panels a and b of Figure 2 show the representative TEM images of the heterostructures. Typically, the inner SiC wires with a diameter less than 50 nm are tightly wrapped by the outer uniform, tens of nanometers thick, SiO_2 layers. An example of a SiO_2 layer with a uniform thickness of ∼12 nm is presented in Figure 2d. As seen in Figure 2a−d, the inner SiC nanowires show obvious contrast variations, either periodic, along the growth direction, or inclined with respect to it. Such variations suggest some planar defects existing within the nanowires, which are visible on a TEM image (Figure 2 d). The period for these defective areas is irregular, normally in the range of 100−500 nm (Figure 2b). The defects were identified as stacking faults formed during the nanowire growth along the (111) plane. A magnified TEM image in Figure 2d indicates that the stacking fault area exhibits a specific fading-away contrast, which is a typical characteristic of a stacking fault, whereas the defect-free area shows no such contrast. The majority of SiO_2 nanotubes were completely filled with SiC nanowires to organize dense core−shell heterostructures, but there were also a small number of them only partially filled (Figure 2d) or fully empty (Figure 2e). The tip-ends of the encapsulated SiC nanowires are atomically flat, suggestive of the layer-by-layer growth along the ⟨111⟩ direction.

To determine the elemental composition and spatial Mn distribution within the SiC/SiO_2 nanocables, chemical composition analysis was consecutively performed on SiC-filled core−shell heterostructures, hollow SiO_2 tubes, and selected catalyst particles by using an energy dispersive X-ray spectrometer (EDS) attached to TEM. The results are presented in Figure 3a−c. One can immediately see the compositional difference for the regarded three cases. Figure 3a is a representative EDS spectrum recorded from an individual SiC/SiO_2 nanocable. To exclude the X-ray counts originating on a supporting carbon film, the spectrum for the SiC/SiO_2 core−shell nanowire that resided far away from the film was taken and quantified. One can see that only Si, C, O, and Cu peaks (the latter originate from a TEM copper grid) are visible for the core−shell wire. No Mn peak was detected within the present EDS resolution, implying that Mn atoms might not penetrate into SiC lattices through Si substitution. The molar ratio between C, Si, and O matches well the overall composition of $SiC:SiO_2 = 1:1$. Similarly, an EDS spectrum obtained from a hollow SiO_2 nanotube also proves the absence of a Mn peak (Figure 3b). The composition analysis performed on a catalyst particle indicates that it consists of O, Si, and Mn (Figure 3c). The results also confirm that an alloy, rather than pure Mn particle, promotes the SiC/SiO_2 nanocable growth, as observed in SEM images (Figure 1). A similar growth phenomenon was also verified for SiC/SiO_2 nanocables with the Fe and In−Ge alloy particles as catalysts.[16−18]

Panels a and b of Figure 4 show representative high-resolution transmission electron microscope (HRTEM) images of a SiC/SiO_2 nanocable. Stacking faults inclined with respect to the structure axis and stretched over the whole wire at an angle of ∼70.5° (with respect to the (111) plane) could be clearly observed. A HRTEM image shown in Figure 4b reveals that the inner SiC nanowire is crystalline and the *d*-spacing between the neighboring fringes perpendicular to the growth axis is ∼0.254 nm. This matches well the $(\bar{1}1\bar{1})$ and $(11\bar{1})$ plane separations of a cubic SiC. An electron diffraction (ED) pattern, displayed in the inset of Figure 4b, further confirms that the wires grow along the ⟨111⟩ direction and the stripes linking the diffraction spots correspond to the stacking faults within the {111} planes. These structural defects are mainly attributed to the thermal fluctuations during the growth. The total system energy usually has a close relationship with the surface and interface of the nanowires.[8] The instability of the system temperature would introduce strains and defects during the crystal growth and lead to the formation of stacking faults on the {111} facets. The outer amorphous SiO_2 layer having a uniform wall thickness of 10−30 nm is chemically inert and thus plays the role of an oxidation protector and thermal insulator for the inner SiC nanowires.

A novel peapod-like structure of SiO_2 tubes encapsulating particles was also observed, as demonstrated in Figure 5b. The latter resembles the previously predicted structure for a Mn-stabilized Si tube, Figure 5a.[14] The inner particles have a uniform diameter of ∼200 nm and are periodically separated at a distance of 300−500 nm. Chemical composition analysis indicates that they are made of Mn, Si, and O, Figure 5d. The Mn−Si alloy particles are crystalline and their structure could be indexed to the orthorhombic structure of a $Mn_{81.5}Si_{18.5}$ phase. In fact, the lattice constants are in good agreement with the XRD data (see JCPDs card 710632). The *d*-spacings of 0.34 and 0.395 nm shown in Figure 5e correspond to the $(32\bar{1})$ and $(\bar{2}11)$ plane separations, respectively. In this case, the outer SiO_2 tube has a thin wall, ∼10 nm thick, and a rough surface, as confirmed by the SEM images (Figure 1d). Figure 5c shows that a SiO_2 tubular structure encapsulating a nanorod is open at one end. Chemical composition analysis performed on the rod concludes that it has the same composition as the embedded particles, Figure 5b. Theoretically, Si nanotubes without metal doping

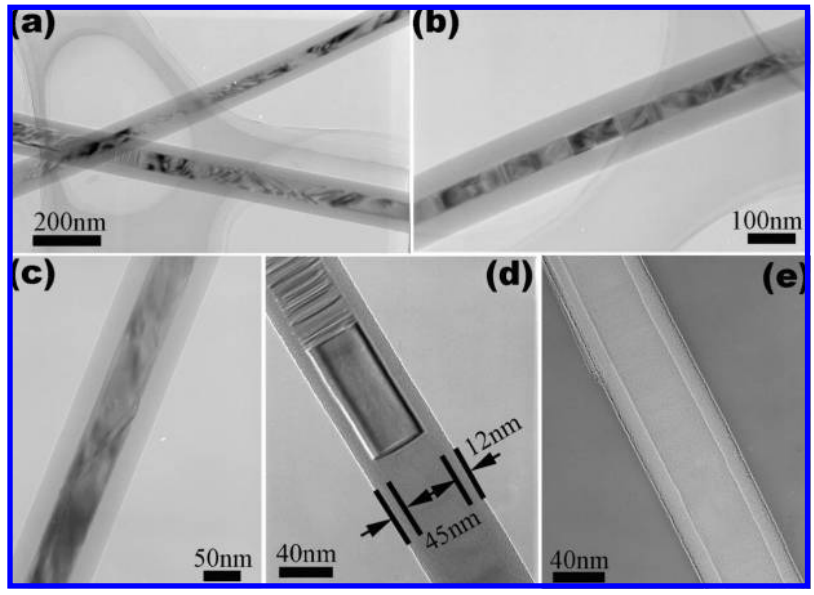

Figure 2. (a, b) Representative low-magnification TEM images of SiC/SiO_2 core−shell structures with uniform diameters and wall thicknesses of the SiO_2 shells. The contrast difference highlights the stacking faults along the (111)plane: (c) completely and (d) partially filled SiC/SiO_2 core−shell heterostructures; and (e) an empty SiO_2 tubular structure.

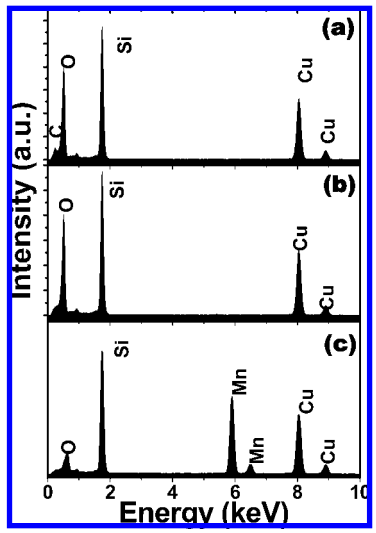

Figure 3. EDS results for (a) a SiC/SiO_2 core−shell heterostructure, (b) a hollow SiO_2 nanotube, and (c) a Mn−Si catalyst particle.

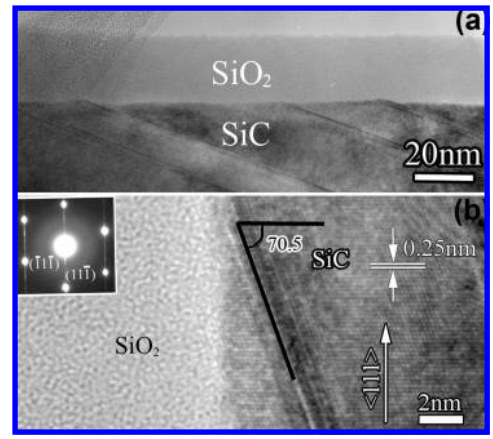

Figure 4. (a) A magnified TEM image of a SiC/SiO_2 core−shell nanocable with stacking faults and a thin amorphous silica layer; (b) typical HRTEM lattice image of a SiC/SiO_2 core−shell heterostructure; the inset is an ED pattern taken along the [011] zone axis. The *d*-spacing of 0.25 nm corresponds to the {111} lattice plane separations for SiC.

would be unstable due to preferential sp^3 Si bonding, while the sp^2 bonding stabilized by metal encapsulation creates a possibility of tubular structure formation.[19] On the basis of the theoretical results, formation of the peapod-like silica tubular structures with encapsulated Mn−Si alloy particles may be described in two steps. First, the Mn−Si alloy particle self-assemblies fill the Si tubular structures, thus forming peapod-like objects, Figure 5b; and second, due to the oxygen present in the reaction chamber, the as-formed Si tubular layers are quickly oxidized to an amorphous SiO_2 shield at a high temperature.

Interestingly, in the present work the catalyst particles were found to be not pure Mn metals but Mn−Si alloys. This is different from the case of SiC nanowires catalyzed by Fe and Ni metals.[11,12] From the Mn−Si alloy phase diagram, one can see that Mn should react with Si to form a binary Mn−Si liquid phase when the temperature surpasses 1280 °C. In this work, the growth temperature (1600 °C) was much higher than that. Therefore, the Mn evaporated from a MnO_2 powder (535 °C) may combine with Si and SiO_2 to form numerous liquid Mn−Si alloy droplets which deposit on the graphite substrate surface in a lower temperature zone. After the formation of such droplets, the flows of Si and C atoms coming from the source powders are absorbed on their liquid surfaces stimulating the continuous growth of SiC nanowires. On the other hand, the Mn−Si droplets can also be easily oxidized due to the oxygen present in the reaction chamber. This process forms the outer SiO_2 layers due to the high bond energy of Si−O.[20] Alternatively, formation of the outer SiO_2 layers can also result from the simultaneous reaction between Si vapor and oxygen in the chamber. It should be noted that the outer SiO_2 tubular layers possibly have a relatively faster growth rate than the inner SiC nanowires. When the Si and C sources were exhausted out, only partially filled SiO_2 tubes were left, Figure 2d.

It is worth noting that SiC nanowires synthesized by catalyst-assisted methods have frequently been reported in the previous works, in which Fe, Ni, or Fe−Co alloy particles were adopted.[12,13,21] GaAs nanowires catalyzed by Mn particles have been proved feasible, but other nanostructures including SiC nanowires with Mn as a catalyst have never been reported.[22]

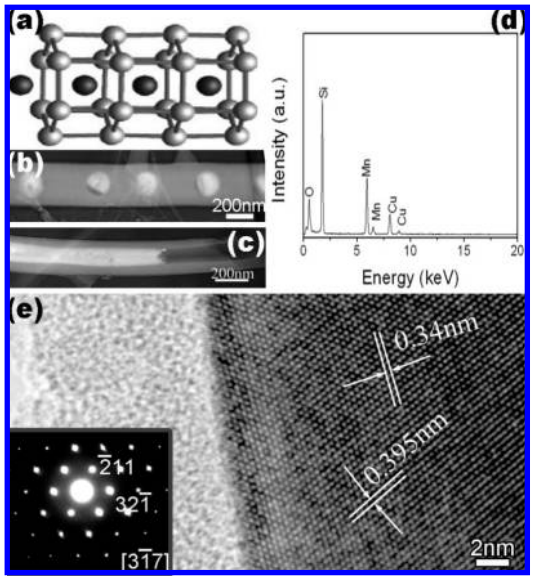

Figure 5. Schematic structure of a Mn-doped Si tube:[14] (b, c) TEM images of a peapod-like SiO_2 tubular structure encapsulating Mn−Si particles and a SiO_2 tubular structure with the broken tip, and filled with a Mn−Si rod; (d) EDS recorded from Mn−Si particles or rods encapsulated into SiO_2 tubes; (e) HRTEM image of a Mn−Si rod shown in panel c; the *d*-spacings of 0.34 and 0.395 nm correspond to the $(32\bar{1})$ and $(\bar{2}11)$ plane separations, respectively. The inset is the ED pattern recorded along the $[3\bar{1}7]$ zone axis.

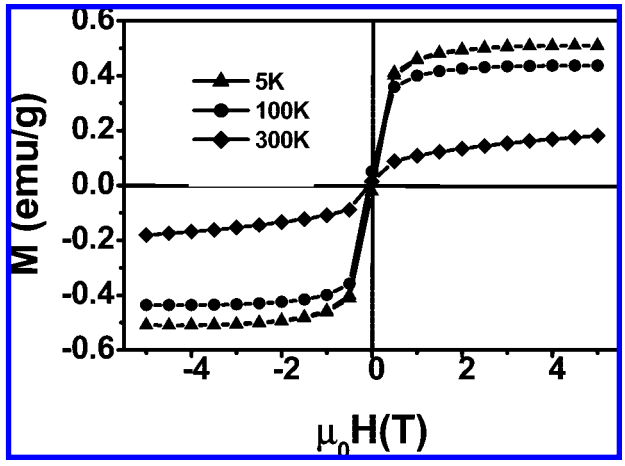

Figure 6. Magnetization curves for Mn−Si-catalyzed SiC/SiO_2 core−shell heterostructures measured at 5, 100, and 300 K. The applied magnetic field ranged from −7 to 7 T.

Figure 6 shows the magnetization behavior of novel Mn-assisted-grown nanocables at various temperatures. Surprisingly, the products were always found to be ferromagnetic in the temperature range from 5 K to room temperature. The saturation magnetization of Mn−Si catalyzed SiC/SiO_2 nanocables exhibits obvious decreasing tendency when a temperature increases from 5 to 300 K. The magnetization decreases from 0.51 emu/g at 5 K to 0.18 emu/g at 293 K. The ferromagnetic behavior of SiC/SiO_2 nanocables can also be confirmed from a thermomagnetic curve measured under a weak field of 100 Oe (Figure 7). Since the Si atoms do not display ferromagnetism and the Mn atoms are usually antiferromagnetically coupled, the origin of the unusual ferromagnetism for the present nanocables is of interest. It has been computed that Mn atoms could be ferromagnetically coupled with neighboring Mn atoms in a Mn-stabilized Si nanotube and that such atoms might have a high local magnetic moment, as high as 3.6 μ_B.[14] Furthermore, on the basis of the

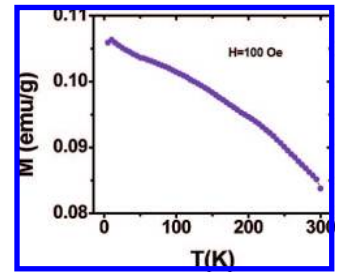

Figure 7. Thermomagnetic curve recorded under a field of 100 Oe with temperature ranging from 5 K to room temperature.

theoretical calculations, it was found that the suppression of hybridization between Mn d states and the sp states of Si in a Mn-doped Si tubular structure might lead to an increase in magnetic moment due to an increase of the Si−Si and Mn−Si bonding lengths.[14] In the present case, though the majority of Mn atoms are incorporated into the Mn−Si alloy particles at the heterostructure tips or encapsulated into their cavities, we consider that some of the Mn atoms could still exhibit ferromagnetic coupling and interact with neighboring Si atoms within the Mn−Si alloy particles, in accord with the theoretical expectations for the peapod-like Mn-doped Si tubular structures. Different from Mn-doped semiconductor nanowires,[23−25] Mn-induced ferromagnetism in SiC/SiO_2 nanocables was strictly limited to nanoscale Mn−Si alloy particles or rods that formed at the starting tips, whereas the SiC-SiO_2 core−shell structures far from the tips and free of Mn doping do not possess any ferromagnetism. This effect is due to the outer thin SiO_2 layers which perfectly serve as an electrical and thermal insulator and protect the inner SiC nanowires from oxidation and chemical erosion in the vicinity of the structure tips which then display local ferromagnetism.

The peculiar core−shell structures, as well as selected area room temperature ferromagnetism, make the present SiC/SiO_2 nanocables valuable for novel magnetic nanodevices. For instance, the randomly grown SiC/SiO_2 nanocables with ferromagnetic Mn−Si particles attached to the tip-ends can be further aligned under an applied magnetic field. Such aligned SiC/SiO_2 can be highly valuable for the fabrication of SiC-based nanoceramics and this is the subject of our ongoing work. In addition, the new peapod-like structures with Mn−Si particles encapsulated into SiO_2 tubular cavities should promote a further intense search for intriguing crystalline Si tubular structures stabilized by transition metals and exploration of their potential applications in spintronics.

4. Conclusion

In summary, Mn−Si-catalyzed SiC/SiO_2 core−shell structures have been synthesized via a simple thermal evaporation process. This is the first example of effective usage of Mn as a catalyst for the SiC/SiO_2 nanocable growth. Different from Mn-doping in other semiconductor nanowires, the present experiments confirmed that Mn atoms are solely located at the tip-end Mn−Si particles rather than dope the nanowire bodies. Magnetic measurements indicated that the nanocables exhibit room temperature ferromagnetism. This behavior was spatially limited to the heterostructure zones in the vicinity of the Mn−Si-alloy containing tip-ends and may be of interest for a design of novel nanoscale spintronic devices. In addition, novel peapod-like silica tubular structures with Mn−Si particles periodically embedded into the tube cavities were discovered. The latter morphology resembles the Mn-doped Si tubes, stability of which was theoretically predicted but never observed experimentally.

Acknowledgment. B.L. would like to thank Drs. Y. Uemura, A. Nukui, C. Y. Zhi, and X. S. Fang of the National Institute for Materials Science (NIMS) in Japan for technical support and kind help in the course of this work. The work was partially supported by the World Premier International Center for Materials Nanoarchitectonics (MANA) Project tenable at the National Institute for Materials Science (NIMS), Tsukuba, Japan.

References and Notes

(1) Suenaga, K.; Colliex, C.; Demoncy, N.; Loiseau, A.; Pascard, H.; Willaime, F. *Science* **1997**, *278*, 653–655.
(2) Yin, L. W.; Bando, Y.; Zhu, Y. C.; Golberg, D.; Li, M. S. *Adv. Mater.* **2004**, *16*, 929–933.
(3) Zhu, Y. C.; Bando, Y.; Yin, L. W. *Adv. Mater.* **2004**, *16*, 331–334.
(4) Wong, E. W.; Sheehan, P. E.; Lieber, C. M. *Science* **1997**, *277*, 1971–1975.
(5) Wu, Y. J.; Wu, J. S.; Qin, W.; Xu, D.; Yang, Z. X.; Zhang, Y. F. *Mater. Lett.* **2004**, *58*, 2295–2298.
(6) Ho, G. W.; Wong, A. S. W.; Kang, D. J.; Welland, M. E. *Nanotechnology* **2004**, *15*, 996–999.
(7) Keller, N.; Huu, C. P.; Ehret, G.; Keller, V.; Ledoux, M. J. *Carbon* **2003**, *41*, 2131–2139.
(8) Tang, C. C.; Bando, Y.; Sato, T.; Kurashima, K.; Ding, X. X.; Gan, Z. W.; Qi, S. R. *Appl. Phys. Lett.* **2002**, *80*, 4641–4643.
(9) Wu, Y.; Yang, P. *J. Am. Chem. Soc.* **2001**, *123*, 3165–3166.
(10) Yang, Y. H.; Wu, S. J.; Chiu, H. S.; Lin, P. I.; Chen, Y. T. *J. Phys. Chem. B* **2004**, *108*, 846–852.
(11) Dick, K.; Deppert, K.; Larsson, M. W.; Märtensson, T.; Seifert, W.; Wallengerg, L. R.; Samuelson, L. *Nat. Mater.* **2004**, *6*, 380–384.
(12) Zhang, Y.; Wang, N.; He, R.; Chen, X.; Zhu, J. *Solid State Commun.* **2001**, *118*, 595–598.
(13) Xing, Y. J.; Hang, Q. L.; Yan, H. F.; Pan, H. Y.; Xu, J.; Du, D. P.; Xi, Z. H.; Xue, Z. Q.; Feng, S. Q. *Chem. Phys. Lett.* **2001**, *345*, 29–32.
(14) Singh, A. K.; Biere, T. M.; Kumar, V.; Kawazoe, Y. *Phys. Rev. Lett.* **2004**, *91*, 146802−1-4.
(15) Shen, G.; Bando, Y.; Zhi, C.; Golberg, D. *J. Phys. Chem. B* **2006**, *110*, 10714.
(16) Li, Y. B.; Bando, Y.; Golberg, D. *Adv. Mater.* **2004**, *16*, 37–40.
(17) Hu, J. Q.; Meng, X. M.; Jiang, Y.; Lee, C. S.; Lee, S. T. *Adv. Mater.* **2003**, *15*, 70–73.
(18) Liu, C.; Li, R. W.; Belik, A.; Golberg, D.; Bando, Y.; Cheng, H. M. *Appl. Phys. Lett.* **2006**, *88*, 043105-1-3.
(19) Singh, A. K.; Kumar, V.; Briere, T. M.; Kawazoe, Y. *Nano Lett.* **2002**, *11*, 1243–1248.
(20) Lange, N. A. *Lange's Handbook of Chemistry*, 11th ed.; Dean, J. A., Ed.; McGraw-Hill: New York, 1973; Chapter 3.
(21) Zhu, Y. Q.; Hu, W. B.; Hsu, W. K.; Terrones, M.; Grobert, N.; Hare, J. P.; Kroto, H. W.; Walton, D. R. M.; Terrones, H. *J. Mater. Chem.* **1999**, *9*, 3173–3178.
(22) Martelli, F.; Piccin, M.; Bais, G.; Jabeen, F.; Ambrosini, S.; Rubini, S.; Franciosi, A. *Nanotechnology* **2007**, *18*, 125603.
(23) Liu, B.; Bando, Y.; Tang, C.; Golberg, D.; Yamaura, K.; Takayama-Muromachi, E. *Chem. Phys. Lett.* **2005**, *405*, 127–130.
(24) Han, D. S.; Park, J.; Rhie, K. W.; Kim, S.; Chang, J. *Appl. Phys. Lett.* **2005**, *86*, 032506−1-3.
(25) Liu, J. J.; Yu, M. H.; Zhou, W. L. *Appl. Phys. Lett.* **2005**, *87*, 172505−1-3.

JP807012K